Comparison of numerical and experimental results for an electrostatic precipitator

Andreas Bäck
Alstom Power Sweden AB
Växjö, Sweden
andreas.back@power.alstom.com

Joel Cramsky
Alstom Power Sweden AB
Växjö, Sweden
joel.cramsky@power.alstom.com

1 Summary / Abstract:

Some fundamental aspects of the electrostatic precipitator are investigated via a combination of tests in a high-voltage rig and numerical computations. The electric field and charge distribution in the duct are computed numerically using the commercially available FEM solver Comsol Multiphysics. The derived properties are compared with experimental data and general operating experience. Overall the agreement between numerical results and experiments is very satisfactory. This provides insight in some basic phenomena governing the precipitator behaviour, and may give qualitative guidance also in the practical design of precipitators.

2 Introduction

The numerical treatment of the electric field and charge distribution within an energized electrostatic precipitator (ESP) has traditionally attracted significant interest. Provided that the boundary conditions at the corona discharge can be simplified the problem formulation is relatively uncomplicated in it's most basic form, despite the fact that the coupled partial differential equations (PDE's) are non-linear. The complexity may then be increased if more advanced geometries and corona models are considered, or if coupling to the gas flow through the ESP is included in the scope. Also time-dependent problem formulations have been studied, for example to simulate a pulsed power supply. Many aspects of the duct-type precipitator have been investigated numerically in previous works and in addition analytical expressions have been developed within certain approximations. A full review is, however, outside the scope of this paper.

The aim of the present work is to demonstrate the possibility to explain some fundamental phenomena appearing in the ESP via solution of the governing differential equations. This is done numerically using the commercially available program Comsol Multiphysics (version 4.1) [1]. This is a user-friendly FEM software package aimed towards coupled systems of partial differential equations. It also includes necessary features for post-processing, including functionality for clear visualisation of the results.

Experimental results have been obtained via an ESP pilot in the high-voltage rig at the Alstom Environmental Control Systems laboratories in Växjö, Sweden. By this test facility comparisons between numerical solutions and actual data was possible. Although the ESP set-up is a "cold pilot" (no hot or dust laden flue gases), care has been taken to reproduce all design details used in an actual commercial ESP. Furthermore the physical dimension is large enough to avoid excessive boundary effects and allow the transformer-rectifier set to operate at a reasonable current level.

3 Numerical

In a steady state situation there is a constant flow of charge (i.e. ions) from the discharge electrodes towards the collecting plates. Neither the electric field nor the charge density changes with time, meaning that the ESP is supplied by an ideal DC supply without ripple or pulsing. For this time-independent approach the equations to be solved are Poisson's equation for the electric field and the continuity equation for charge conservation:

$$\nabla \cdot \varepsilon_0 \mathbf{E}(\mathbf{x}) = \rho(\mathbf{x}) \text{ and } \nabla \cdot (K \rho(\mathbf{x}) \mathbf{E}(\mathbf{x})) = 0$$

Here $\mathbf{E}$ is the electric field and ρ is the charge density, while K is the mobility of the charge carriers. ε_0 is the permittivity of free space. The position vector $\mathbf{x}$ corresponds to (x, y, z) in

the general 3D case. In practice the differential equations above are often expressed in terms of the electric potential, $\Phi(\mathbf{x})$, related to the electric field by $\mathbf{E}(\mathbf{x}) = -\nabla\Phi(\mathbf{x})$. The corresponding second order equations are also typically the form that appears in most numerical schemes. The solution of the two equations can either be treated as a fully coupled system directly on the finite element mesh, or by iterative solution of the separate equations until self-consistency is reached.

The basic geometry of a duct-type precipitator is rather straightforward. In fact, a two-dimensional numerical treatment is enough to catch most of the physics related to the electric field and charge transport. Specifically for straight wires as discharge electrodes a 2D geometry is an exact mapping of the full three-dimensional problem. Typically the high degree of symmetry within a duct allows for further simplification of the problem via periodic and mirror boundary conditions around the symmetry cell. This is exemplified in Fig. 1 below, where the most basic geometry is shown together with a solution of Poisson's equation for $\rho = 0$ inside the symmetry cell.

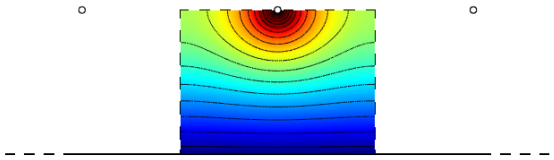

Fig. 1: Basic 2D geometry for duct-type ESP. The domain treated numerically is shown with a solution for the electric potential. The size of the discharge wires has been slightly exaggerated in the figure for the sake of clarity.

Even if the duct-type ESP in it's most basic form it is essentially a 2D problem a full three-dimensional treatment is required for most practical electrodes or if top/bottom boundary effects are studied. An inherent complication is the small size, or curvature, of the corona-generating region of any discharge electrode, compared to the spatial extension of the inter-electrode volume. This can, however, be overcome by a proper selection of adapted mesh for the FEM discretization.

For solution of the partial differential equations boundary conditions are needed within the specified geometry. Two of these, for the potential Φ, are straightforward Dirichlet conditions. The grounded collecting plates gives $\Phi = 0$, while the potential at the discharge electrode is taken as the ESP operating voltage ($\Phi = -U$). However, a boundary condition is also needed for the charge density, ρ, and this is a matter of some complexity. The physics of the corona discharge, which generates the charge carriers at the discharge electrode, is so complicated that a detailed treatment is in principle out of the question. Instead some form of phenomenological ad-hoc model must be utilized at the discharge electrode boundary to capture as much as possible of the behaviour. In general a non-linear boundary condition, where the charge density at the discharge electrode depends on the electric field, is required for a realistic treatment (simulation) of the (actual) corona discharge. This may for example be the Peek condition for corona onset, postulating that above a critical field strength, E_{ON}, the charge density at the discharge electrode becomes non-zero [2]. As the voltage is raised, the charge density at the boundary has to increase correspondingly in such a way that the charge supplied to the domain balances the electric field to stay at E_{ON} (Kaptzov's assumption). This is especially easy to accomplish in a 2D model with symmetrically positioned wires, since the field strength around the wire surface is virtually constant.

The main tool for the numerical computations in this work is Comsol Multiphysics [1]. This a FEM software package for various physics and engineering applications, especially coupled phenomena. The entered equations and boundary conditions are collected into one large system that is solved using a weak formulation. Comsol has a selection of direct- and iterative finite element solvers for stationary problems, as well as advanced solution methods for time-dependent equations. All computations in the present work were performed on a standard PC, equipped with 24 Gb RAM and a six-core Intel Xeon 5650 processor at 2.66 GHz.

To back up the results from Comsol they have been compared against corresponding solutions from a program developed by Alstom in the 90's specifically for numerical ESP simulations [3-5]. Furthermore, three different numerical schemes within Comsol itself were compared for the same bench scale problem, as a further consistency check. Figure 1 show results from one such comparison. The electric potential, Φ, and charge density, ρ, are plotted along a line that goes straight from the

discharge wire directly towards the collecting plate surface. The ion mobility, K, is assumed to be 1.8×10^{-4} m^2/Vs [6].

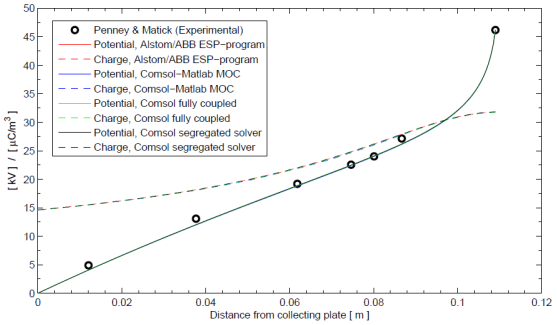

Fig. 2: Comparison of numerical schemes from Comsol and old ESP-program. Black circles represent experimental data by Penney-Matick

By choosing the collecting plate spacing, wire pitch and wire radius in the ideal geometry to 9'', 6'' and 0.04'', respectively, the numerical solution for the electric potential could also be compared against experimental results by Penney and Matick [7]. The applied voltage is 46.2 kV. It is seen from Figure 2 that all numerical schemes generate identical results (indistinguishable curves), and that the potential is in excellent agreement with the measured data. It is also worthwhile to mention that the Penney-Matick experiments gave an average current density of 688 μA/m^2 for the voltage at hand, while the computations result in 725 μA/m^2. The relatively good agreement indicates that also the charge density from the computations may be representative of the real situation.

For the computations seen in Figure 2 the value of the critical field strength, E_{ON}, has been taken as 6.1×10^6 V/m, which follows directly from Peeks formula [2] for ambient temperature and a wire radius of 0.04''. The charge density at the corona wire has then been selected so as to keep the electric field constant at this value around the wire surface, in accordance with Kaptzov's assumption. Given the good agreement of the computations with experimental data this treatment of the boundary condition seem to be suitable (satisfactory), at least for the type of 2D geometries suitable for a duct-type precipitator.

A further feature of the numerical model has also been added to the Comsol computations from here on, namely the inclusion of ion diffusion. This means adding the diffusion term $-D\,\nabla^2\rho(\mathbf{x})$ to the left hand side of the continuity equation. Including diffusion in the model makes it scientifically more correct and even though the diffusion constant, D, is a small number it has been claimed that the agreement with experiments becomes better [8]. Diffusion also contributes to stability in the numerical computations.

4 Experimental set-up

To be able to compare the numerical results against actual experimental data an ESP set-up has been constructed. It consists of two parallel gas passes that can be fitted with either helical wires (spirals) or straight wires as discharge electrodes. Each collecting electrode curtain consists of four profiled plates with a nominal width of 800 mm (i.e. resulting in a field length of 3.2 m). The height of the collecting plates is 4 m, leading to a collecting area of 51.2 m^2. The wire/spiral diameter is 2.7 mm, leading to $E_{ON} = 5.7\times10^6$ V/m.

Since one of the purposes of the ESP test-rig is to investigate critical areas for spark-over, it is constructed as a replica of a standard Alstom commercial precipitator. Thus, even if it is a cold pilot, it includes details like shock bars, tumbling hammers and rapping shafts.

The ESP can be energized either by a conventional transformer-rectifier (T/R) or by a high frequency power converter (SIR). The conventional single-phase T/R is rated 200 mA and 200 kV$_p$. The SIR (Switched Integrated Rectifier) converts a three phase AC at the mains to a rectified high frequency, high voltage output [9]. This leads to nearly perfect DC current, compared to the rippled DC from a conventional T/R. The rating of the particular SIR used for the ESP rig is 200 mA, 125 kV$_p$.

Fig. 3: View of the ESP set-up in the HV-rig with the side cover removed to expose the collecting plates.

The latest feature added to HV-rig is the possibility to measure the current distribution profile on the collecting plate. The data generated by this equipment is compared against numerical results in Section 5.3. Similar current distribution measurements have also been performed previously in the Alstom high voltage lab. A well-distributed current is of importance e.g. to minimize back-corona in a real precipitator [10].

5 Results

A selection of results from the numerical Comsol computations of relevance for a practical precipitator are described in the below sections. Where possible the numerical results have been compared to experimental data or general field experience. Although voltages and charges are given as absolute numbers, negative corona is implied throughout.

5.1 Profiled collecting plates

To reach the mechanical stability required for a tall collecting plate it must be profiled. Since the electrical field strength at the grounded plate surface is postulated to determine when a spark-over occurs, it is very important to have smooth curvatures [11].

Comsol has functionality to import CAD drawings, which was convenient for building the geometry for the plates. Compared to the ideal geometry the number of mesh points increases significantly at the plate to be able to resolve the electrical fields at the G-profiles at the end of the plate. Furthermore, the symmetry cell now includes all three wires and both collecting plates. This can be appreciated from Figure 4, where the electric field strength is shown as a colour map.

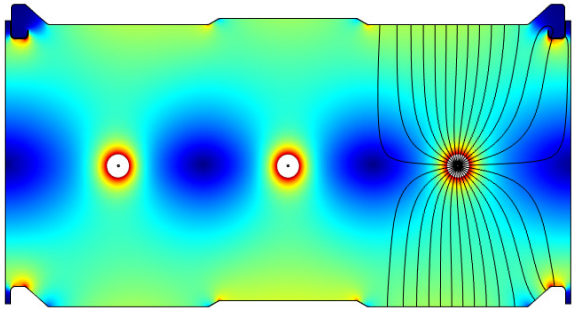

Fig. 4: Electric field intensity of a solution with profiled 800 mm collecting plates. For the rightmost wire also the field lines are included.

It can be seen in figure 4 that the electric field is significantly enhanced at the perturbations on the collecting plates, in accordance with previous findings [8]. When comparing the computed maximum field strength at the G-profiles for a current matching the spark-over limit in the experimental rig, it was found that it was virtually independent of e.g. plate spacing. Thus, the combined results from numerical computations and experimental spark-over voltages support the assumption that it is indeed the maximum local electrical field strength at the grounded plates that determines the spark limit in a precipitator. This critical field strength, occurring at the upper G-profiles to the left and right in Figure 4, was 1.2×10^6 V/m.

5.2 Voltage-Current characteristics

An important diagnostic of a precipitator is the current-voltage characteristics, or I-V curve. The reproduction of an I-V curve within the numerical treatment of an ESP is thus an important consistency check of any model.

Figure 5 compares experimental I-V curves generated by both the conventional T/R and the SIR power supply with computed curves from Comsol. Also the difference in I-V characteristics between spirals and straight wires obtained in the test-rig is shown (for the SIR power supply). The experimental data shows that for a given average current input the average voltage is somewhat higher for the SIR compared to the conventional T/R. However, the peak voltage for a given current is significantly higher for the conventional T/R due to the ripple. For example, at an average voltage of 70 kV_{av} the peak voltage was measured to be 110 kV_p for the T/R. For the SIR the corresponding value was about 75 kV_p. From this it is easily understood that a significantly higher power input can be reached before spark-over. Another finding from the HV-rig is that the voltage is about 6 kV higher for straight wires compared to spirals for any given current.

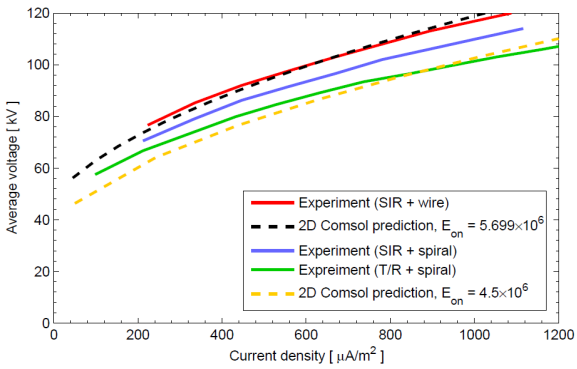

Fig. 5: Comparison of experimental and numerical I-V curves. The collecting electrode spacing is 500 mm.

The numerical results, shown as dashed lines in Figure 5, demonstrate that the best agreement between the computations and experiments is obtained for the straight wires and SIR. This is expected since the numerical model for this case is the straight wires (2D) and perfect DC current (stationary model). The significant time dependence due to the 50 Hz ripple from a T/R cannot be properly represented in our stationary numerical treatment. Therefore it is seen that even when the corona onset from Peek's experiments is artificially lowered by as much as 20% the curve shape does not fit the data obtained from the T/R very good. ((When changing from spirals to wires in the experiments, the SIR characteristics get much closer to the computations that are based on E_{ON} taken from Peek's formula.))

5.3 Current distribution on the collecting plates

A special foil glued to one of the collecting plates in the HV-rig allows measuring the current entering each cm^2 of the collecting area. Corresponding information can easily be obtained from the post processing tools for a numerical solution in Comsol. A comparison between an experimental measurement and a numerical computation at an average current desity of 600 µA/m^2 is provided in Figure 6.

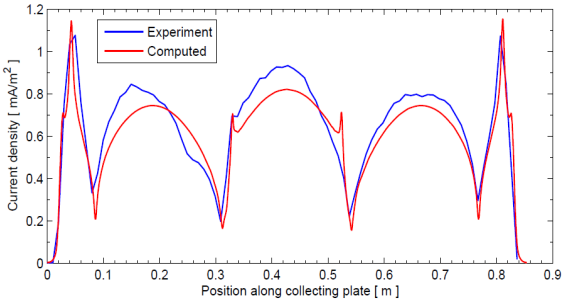

Fig. 6: Profile of the current entering the collecting plate with straight wires.

The agreement between experiment and computation is seen to be quite good. The three "humps", showing the higher current density in front of each spiral are well reproduced, as is the sharp peaks at the G-profiles at the edges of the collecting plates. The high current at the plate perturbations is a direct reflection of the high electrical field strength at these positions (c.f. Figure 4). Since straight wires were used for the experiment the 2D treatment in Comsol suffices for an exact representation of the actual geometry.

5.4 Estimate of migration velocity

The classical measure of ESP performance is the Deutsch migration velocity, ω, which may be seen as the speed at which the particles travel towards the collecting plates [12]. The ESP collection efficiency is then given by $1-C_{out}/C_{in}=\exp[-\omega A/Q]$, where A/Q is the specific collecting area in m^2/m^3/s. The equilibrium velocity of a charged particle of radius a in the electric field is given as the balance of the driving force and the drag force: $q\,\mathrm{E}_y = 6\pi\eta a\,\omega$.

The electrical charge on the particle at saturation can be estimated in the field charging regime by $q=12\pi\varepsilon_0 a^2\|\overline{\mathbf{E}}\|$ [12].

From the numerical solution the electric field is known at each point in the inter-electrode space. Assuming that the turbulence and gas flow gives no net contribution to the transport of a particle towards the collecting plates, the average velocity is given by:

$$\omega=\frac{2\varepsilon_0 a}{\eta}\|\overline{\mathbf{E}}\|\int_\Omega d\mathbf{x}\left|\mathrm{E}_y(\mathbf{x})\right|\Big/\int_\Omega d\mathbf{x}.$$

The charging field, $\|\overline{\mathbf{E}}\|$, is taken as:

$$\|\overline{\mathbf{E}}\|=\int_\Omega d\mathbf{x}\|\mathbf{E}(\mathbf{x})\|\Big/\int_\Omega d\mathbf{x}.$$

The integrals can be performed by the post processing tools in Comsol on the solution domain, Ω, for the geometry and boundary condition (voltage) at hand.

Since there has been some debate in the past regarding the influence of plate spacing on migration velocity the evaluation has been done for a number of geometries, having different spacing. The computations have been repeated for several current densities for each spacing. The result is shown in Figure 7.

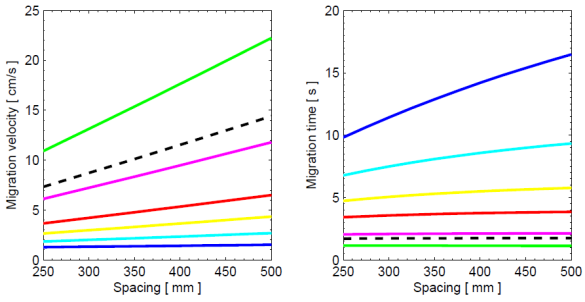

Fig. 7: Migration velocity as function of plate spacing for different current densities. The migration time in the right graph is in principle the velocity divided by half the spacing.

The calculations have been performed for particles of diameter 2 µm ($a = 1\times10^{-6}$) and a gas viscosity, η, of 1.8×10^{-5}. As expected the migration velocity increases with increasing current density (and associated voltage). The curves represent 50, 150, 300, 500, 1000, 1250 and 2000 µA/m^2, respectively. The curves come in the opposite order in the right graph, showing the migration time. The dashed curve, having a current density of 1250 µA/m^2, represents the break line where the migration velocity becomes proportional to the plate spacing. However, already at e.g. 500 µA/m^2 the migration time has a very weak dependence on the spacing.

It is important to emphasize that the above measure for the migration velocity is only a rough qualitative estimate. From the full numerical solution a number of other variants could be envisioned, such as for example limiting the integration to an area adjacent to the collecting plate where the actual collection of particles take place. Another approach that is more advanced is to add also the gas flow inside the ESP, including turbulence models and volume force from the ion transport, and thereafter run particle trajectories through the domain. The fraction of particles that reach the far end of the domain compared to those impacting on the collecting plates gives an estimate of the collection efficiency. However, even the most advanced model would likely not be able to provide a practical estimate of w that may be used e.g. for ESP sizing.

5.5 Impact of space charge due to dust laden gas

The phenomenon of corona suppression due to the space charge effect from a large amount of sub-micron particles in the gas is a well known problem for certain ESP applications, such as soda recovery boilers [13]. Even for "ordinary" applications, as for example precipitation of fly ash after a coal-fired boiler, it is typically seen that the first field of the ESP has to operate at a higher voltage to reach a given set-point for the current. Often this also leads to excess sparking in the front field.

The simplest theoretical model to take into account the dust space charge is to add a constant contribution to the charge density in the entire domain [11,13]. This contribution does not add to the current due to the very low migration velocity of the particles compared to the charge carried by the fast-moving ions. In the simplest approach the addition of dust space charge Poisson's equation thus takes the form $\nabla \cdot \varepsilon_0 \mathbf{E}(\mathbf{x}) = \rho(\mathbf{x}) + \rho_{dust}$, while the continuity equation remains unchanged. When this exercise is done in the numerical 2D model, it is clearly seen how, for a given voltage, the current decreases when ρ_{dust} becomes larger. This is demonstrated in Figure 8 for the voltages 60 kV and 80 kV at a plate spacing of 400 mm.

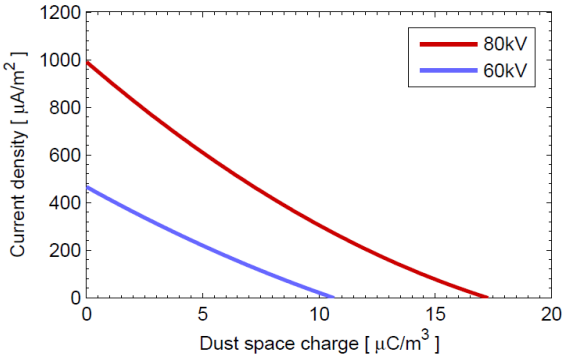

Fig. 8: Current density as function of dust space charge for 60 kV and 80 kV.

It is interesting to note that complete corona quenching occurs already at a dust space charge of 11 µC/m^3 and 17 µC/m^3 for 60 kV and 80 kV, respectively. This is significantly lower than the charge that would be attached to fully saturated particles for typical dust concentrations at the ESP inlet. For example, the virgin fly ash from a pulverized coal boiler may have a surface area in the order of 1 m^2/g. For a typical inlet dust concentration to the ESP of 10 g/m^3 this would result in a saturation charge of >100 µC/m^3 for a reasonable average charging field (c.f. expression in Section 5.4). Thus… Thus By the same token the particles cannot reach their saturation charge before a significant fraction of them have disappeared from the inter-electrode region by precipitation on the collecting plates. Only when a significant fraction of the dust has disappeared from the inter-electrode space can the remaining particles reach their saturation charge.

It is not necessary to limit the dust space charge to a simple constant in the numerical treatment. For example, it can be taken as an arbitrary function along the length of the precipitator, i.e. $\rho_{dust}(y)$. If a reasonable shape is selected for the function this can for example simulate the decrease of ρ_{dust} due to collection of particles.

This was performed for a numerical model with parameters loosely based on recent data from an ESP after a lignite-fired oxyfuel boiler [14]. The function was taken to be of the form $\hat{\rho}\,\theta(y)\exp[-\lambda y]$, where $\theta(y)$ is a smoothed

step function to simulate the charging of the particles, and λ is selected to represent a realistic decrease of the dust (charge) concentration through the first field of the ESP. The maximum dust charge, $\hat{\rho}$, was selected as the charge density for complete corona quench, which is the 11 μC/m^3 from Figure 8 since the operating voltage was around 60 kV for the present example. From dust measurements at the oxyfuel plant it was concluded that the dust concentration after the first ESP field was in the order of 20 mg/m^3 at the high current density prevailing (450 μA/m^2). For this low dust concentration the particles can have their saturation charge without completely quenching the corona. Since the remaining particles have a smaller average diameter a dust space charge of a few μC/m^3, may be expected. Given this an appropriate value for λ can be selected.

The so-obtained function for $\rho_{dust}(y)$ was added to a 2D model stretching over the full length of the first ESP field. The boundary conditions at the wires were to comply with the Peek-Kaptzov assumption. The numerical result showed that the voltage needed to reach the set point of 450 μA/m^2 was 6 kV higher compared to the case when no dust space charge was added. This correlates well with the voltage difference of about 5 kV between the first and second ESP field, which was observed during the measurement campaign at the oxyfuel plant [14].

Of course the selected expression for $\rho_{dust}(y)$ is rather arbitrary, although based on some reasonable assumptions. It is anyhow interesting to see that this ad-hoc approach result in a level of corona suppression that compares favourably with actual observations at site. This being said, it would be desirable to develop a model in which the dust charge is actually a function, $\rho_{dust}(\mathbf{x})$, included in the system of PDE's. In this way it could be appropriately coupled to the ionic charge to reach a fully self-consistent solution. However, since $\rho_{dust}(\mathbf{x})$ is inherently dependent on the dust concentration, assumptions regarding the particle collection would still have to made since it is not realistic to include a model for the dust concentration $C(\mathbf{x})$ in the PDE's.

5.6 3D-computations for spiral discharge electrodes

Although it has been shown by the previous sections that very much of the physics of a duct-type ESP can be adequately covered in a 2D model, some computations have also been carried out in 3D. This was done for the spiral discharge electrode, which is often fitted in real ESPs due to its good current distribution. The 3D-treatment requires a significantly higher number of mesh-elements in the numerical model, making memory and computation time an important factor to consider. It was possible to use about 500 000 mesh elements with a segregated solver for one turn of one spiral with non-profiled plates. About 80% of the mesh points are located in the immediate vicinity of the spiral electrode.

Also the corona model must be treated in a more elaborate way, since the electric field now becomes highly non-uniform on the spiral surface. This being said it was still desired to have a Peek-Kaptzov condition for the corona, given the successful use of this approach for the 2D results. To model the corona discharge by a non-linear boundary condition, where ρ depends on the electric field at the electrode surface, will require some assumptions about the physics. Since it is our intention to avoid this as far as possible we start off with a relation that is as simple as possible:

$$\rho(\mathbf{x}_\Gamma) = \alpha \times \left(\left\| \mathbf{E}(\mathbf{x}_\Gamma) \right\| - E_{ON} \right).$$

It now has to be understood that the Peek-Kaptzov condition will follow when the coefficient α goes towards infinity. Then the corona discharge will act as a copious source of charge and even the smallest increase of the electric field at the boundary will generate the charge needed to quench the field by negative feedback in the self-consistent solution. Due to this the exact functional relationship of the boundary condition becomes relatively insignificant. Unfortunately the problem also becomes increasingly non-linear when α increases, resulting in convergence problems if the numerical scheme is not set up in a correct way.

The boundary condition as per above can be directly implemented in Comsol and the selection of a suitably large value of α was based on comparisons within the already investigated 2D modes. Thus, when α was taken large (about five times the ion mobility) the results sufficiently close replicated those obtained previously with the manually controlled Peek-Kaptzov condition. Further increase of α did then not change the results appreciably.

The geometry and numerical solution for the 3D spiral can be appreciated from Figure 9. From the cut-plane it is seen how the corona discharge is injecting charge to the domain from the "outer" side of the spiral surface,

where the electric field is strongest. The figure also shows the nodal pattern of the current distribution entering the collecting plates, which has been confirmed by measurements [3,10].

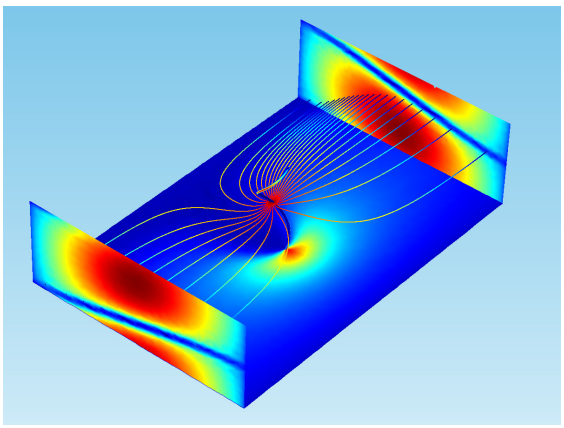

Fig. 9: Computation for 3D spiral with flat collecting plates and periodic boundaries. The current profile on the plates shows the typical nodal pattern.

Regarding the current-voltage characteristics the computations give at hand that the voltage needed for a certain current is about 2 kV lower for a spiral compared to a straight wire. This is in the right direction, but does not replicate the 6 kV seen experimentally in Section 5.2. Reasons for the discrepancy could be details of the corona model as well as the non-profiled collecting plates used for the numerical treatment of the spiral (profiled plates have been seen to increase the current input by 4-5% within the 2D model).

6 Conclusions

By a number of examples it has been shown that numerical computations can be used for an increased understanding of various phenomena in the duct-type ESP. For this purpose it is very often enough with a two-dimensional treatment. Satisfactory agreement with experiments and field experience was reached. For the type of investigations performed in the present work it is possible to use commercially available FEM solvers, like Comsol Multiphysics, and regarding the hardware it is nowadays enough with a state-of-the-art PC.

Acknowledgements

The authors would like to thank Jörgen Linnér and Anders Johansson at the Alstom Thermal Service division in Växjö for their invaluable help to set up the SIR rectifier and the current distribution measurements, respectively.

7 Literature

[1] COMSOL Multiphysics - User's Guide; Version: October 2010 COMSOL 4.1

[2] Peek JR, F. W.; Dielectric Phenomena in High Voltage Engineering. 3rd ed.; McGraw-Hill; New York; 1929

[3] Egli, W.; Kogelschatz, U.; Persson, T.; Three-dimensional corona current distribution in complex ESP configurations; ICESP VI; Budapest, Hungary; June 1996

[4] Egli, W.; Kogelschatz, U.; Gerteisen, E. A.; Gruber, R.; 3D computation of corona, ion induced secondary flows and particle motions in technical ESP configurations; Journal of Electrostatics 40&41; 1997; pp.425-430

[5] Kogelschatz, U.; Egli, W.; Gerteisen, E. A.; Advanced computational tools for electrostatic precipitators; ABB Review 4; 1999; pp.33-42

[6] Davis, J. L.; Hoburg, J. F.; Wire-duct precipitator field and charge computation using finite element and characteristics method; Journal of Electrostatics 14; 1983; pp.187-199

[7] Penney, G. W.; Matick, R. E.; Potentials in D-C corona fields; Trans. AIEE 79; 1960; pp.91-99

[8] Abdel-Salam, M.; Al-Hamouz, Z.; Finite-element analysis of monopolar ionized fields including ion diffusion; Journal of Physics D: Applied Physics 26; 1993; pp.2202-2211

[9] Ranstad, P.; Porle, K.; High frequency power conversion: A new technique for ESP energization; EPRI/DOE International Conference on Managing Hazardous and Particulate Air Pollutants; Toronto, Canada; August 1995

[10] Porle, K.; On back corona in precipitators and suppressing it using different energization methods; ICESP III; Abano-Padova, Italy; October 1987

[11] Stomberg, H.; Åkerlund, C-E.; On the influence of field strength in wire-plate electrostatic precipitators with regard to the electrode configuration and dust space charge; Journal of Electrostatics 17; 1985; pp.85-94

[12] White, H. J.; Industrial Electrostatic Precipitation; Addison-Wesley; Reading MA; 1963

[13] Lindau, L.; Matts, S.; Some space charge problems encountered with large electrode spacing; ICESP II; Kyoto, Japan; November 1984

[14] Bäck, A.; Grubbström, J.; Ecke, H.; Strand, M.; Pettersson, J.; Operation of an electrostatic precipitator at a 30 MW_{th} oxyfuel plant; ICESP XII; Nürnberg, Germany; May 2011